Supplementary information

Tryptophan-to-haem electron transfer in ferrous myoglobins

Roberto Monni, Andre Al Haddad, Frank van Mourik, Gerald Auböck and Majed Chergui*

Laboratoire de Spectroscopie Ultrarapide, École Polytechnique Fédérale de Lausanne, FSB- ISIC, CH-1015 Lausanne, Switzerland

SI. Material and Methods

SI.1 Sample preparation

The following doses were used to prepare 100 mL of 0.1 M phosphate buffer: 30 mL of a sodium hydroxide (NaOH) 0.1 M aqueous solution were added to 50 mL of a potassium orthophosphate (KH_2PO_4) 0.1 M aqueous solution, and the mixture was then diluted to 100 mL with 18 mQ distilled water. The KH_2PO_4 solution was prepared by dissolving 0.68 g of the latter in 50 mL of 18 mQ distilled water, while the NaOH solution was obtained by dissolving 0.20 g of NaOH in 50 mL of the same type of distilled water. The pH was controlled by a pH-meter and adjusted, if necessary, with the rest of NaOH solution or by addition of a dilute Hydrochloric acid (HCl) solution (0.05 M). The buffer solution used for the experiments was further diluted to a concentration of 10 mM.

Lyophilized horse heart met-Mb and sodium dithionite ($Na_2S_2O_4$), were purchased from Sigma Aldrich and used as delivered without any further purification. The deoxy-Mb was prepared under inert gas environment, by flowing Argon (Ar) in a portable glove box, to avoid both oxidation of the reagents and consequent formation of the oxy-Mb complex. The met-Mb was flowed with Ar in the glove box for ~30 min and then dissolved in a degased phosphate buffer solution (10 mM) at pH 7. A 2-fold excess of sodium dithionite, with respect to the equimolar ratio, was added to the met-Mb solution to obtain the deoxy-Mb. Figure S1 shows the static absorption spectrum of the deoxy-Mb of a solution of ~0.3 mM in a 0.2 mm-thick cell. This was enough to obtain an optical density of ~0.15 at the excitation wavelength (315 nm or 290 nm). The deoxy-Mb solution was handled and held in an air-tight container with an inlet to introduce a small overpressure of Ar gas during both transportation and the entire measuring time, so as to avoid possible oxygen leaks. The deoxy-Mb's static spectrum (Fig. S1) was checked before and after each experiment to control integrity of the sample.

SI.2 Optical setup

The experiments were performed on a 2D-UV transient absorption setup, which has been described elsewhere.(2, 3) Briefly, ~0.4 mJ of the output of a 20 kHz, cryogenically-cooled, amplifier (Wyvern, KMlabs, 780 nm, 50 fs, ~0.6 mJ) are injected into a Non-collinear Optical Parametric Amplifier (NOPA) (Topas White, Light Conversion) to provide pulses in the visible range between 560 nm and 650 nm. The typical output energy is ~15 μJ and ~60% of it is used to generate narrow-band pump pulses. The visible pulse is focused on a 0.5 mm-thick BBO crystal for frequency doubling, in order to generate UV pump pulses (290 nm and 315 nm) with typical band-width of ~2 nm and energies of ~150 nJ. The latter is chopped at half the laser repetition rate and focused onto the sample with typical spot-size of 110 μm x 110 μm. In our experiments the pump pulse-length was ~200 fs Full Width at Half Maximum (FWHM), leading to an instrument response function (IRF) of ~300 fs FWHM.

The visible probe pulses were generated by focusing ~0.5% (~1 μJ) of the remaining output of the amplifier (~0.2 mJ) onto a 5 mm-thick CaF_2 window, in order to generate a white light super-continuum. The probe region used in our experiments spans from 390 nm to 730 nm, covering the main absorption features of the haem (Soret- and Q-band).(4, 5) After focusing

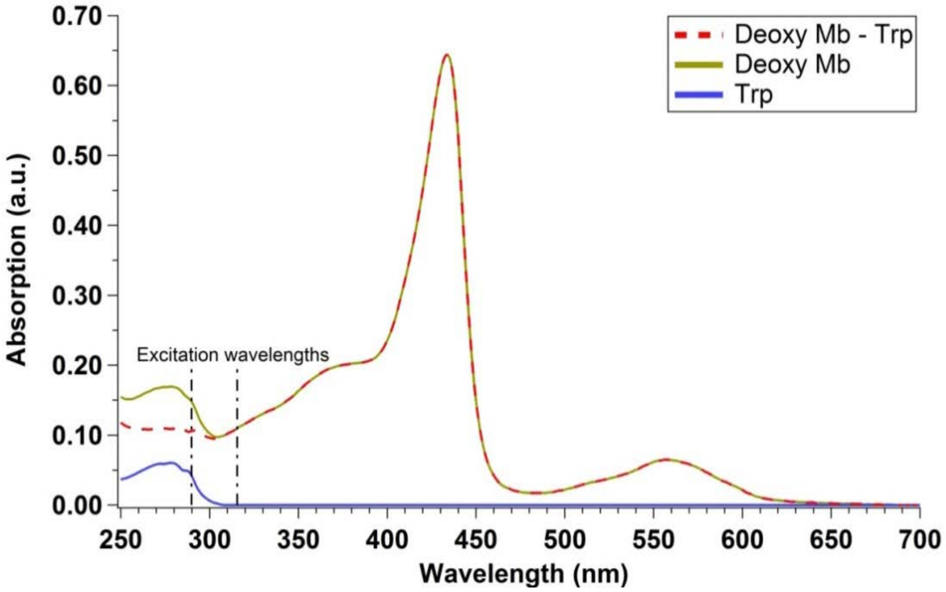

Figure S1: Static spectra of deoxy-Mb 0.27 mM (solid yellow line), Trp in water 0.54 mM (solid blue line) and difference between deoxy-Mb and Trp spectra (dotted red).

onto the sample (30 μm x 30 μm spot-size) the probe is coupled into a 100 μm multi-mode fiber and sent to a spectrometer to be spectrally resolved and detected on a single shot basis by means of a fast CMOS array detector.

SI.3 Power dependence

Figure S2 shows the power dependence of the signal upon 315 nm (Panels A and B) and 290 nm excitation (Panel C). Each point in Figure S2 was obtained by integration of the absolute transient signal in the region between 387 and 580 nm, in order to have a better signal to noise ratio. However, the integration of the absolute value of the signal leads to a positive offset due to integration of the noise of the measurement. The latter does not influence the results of the power dependence since it only adds a rigid shift of each point.

The points were fit using a power law given by

$$y = y_0 + Ax^z \tag{S1}$$

Where y_0 indicates the vertical offset, A is the amplitude of the power law and z is the power of x, which is indicated as "*pow*" in the fit results shown in the insets of Fig. S2.

The power dependence of deoxy-Mb upon 315 nm photo-excitation was measured at two different time-delays, namely 1.5 ps and 600 ps, and the results are reported in Figure S2A and B, respectively. As shown in Figure S2A, at 1.5 ps delay-time the dependence is well described by a fit with z = 1.0 ± 0.1. At 600 ps (Fig. S2B), the fit yields z = 2.5 ± 0.4, implying that this signal is due to a two-photon absorption processes. It is important to note that this quadratic behavior is visible only at long time-delays where only a small signal from

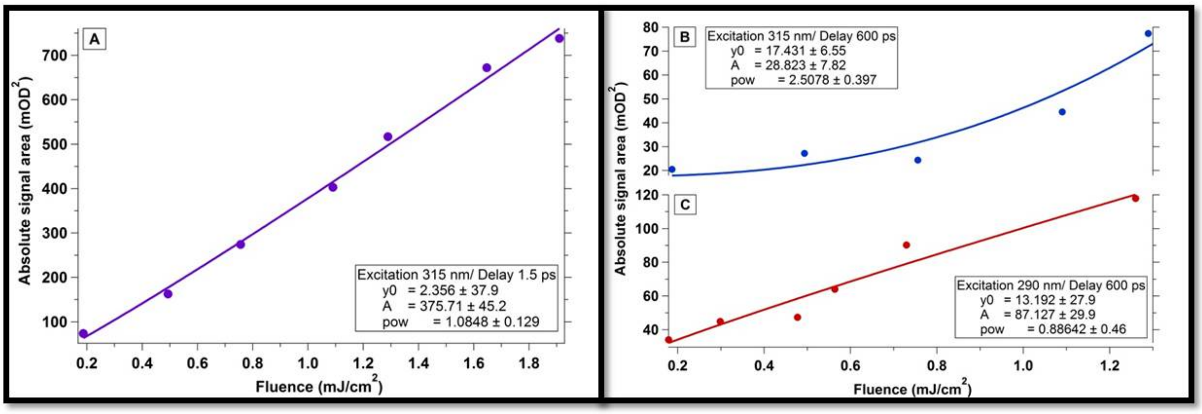

Figure S2: (A) Power dependence of deoxy-Mb upon 315 nm excitation at a pump-probe delay of 1.5 ps. (B) Power dependence upon 315 nm excitation at a pump-probe delay of 600 ps. (C) Power dependence upon 290 nm excitation at 600 ps delay. In each panel the fit coefficients are given.

a long lived photoproduct remains. At short time delays the signal appears linear because the small two-photon signal is covered by a much larger signal resulting from the normal haem photo-cycle.

Figure S2C shows the power dependence at 600 ps pump-probe delay upon 290 nm excitation, in order to concentrate on the long-lived (LL) transient signal resulting from the Trp^{14} to haem electron transfer (see main article). The fit of the power dependence gave $z = 0.9 \pm 0.5$, meaning that the process is linear and not related to multi-photon absorption processes.

As a consequence, we performed the measurements at a fluence of ~0.8 mJ/cm^2 at both excitation wavelengths, which is the best compromise between minimal multi-photon absorption and good signal-to-noise ratio.

SII Results

SII.1 Trp fluorescence quenching times

Table S1 shows the time constants of the Trp^7 and Trp^{14} fluorescence for several Sperm Whale (SW) myoglobin complexes and for horse heart (HH) apo-myoglobin. All Mbs have two Trp residues at positions 7 and 14, at nearly similar distances from the haem.(6, 7) It can be seen that the decay times for the different Mbs do not change dramatically, but that for apo-myoglobin, the decay constant for both Trps are significantly longer and are actually close to those of Trp in water.(8)

Table S1 : Fluorescence decay times (in picoseconds) of Trp^7 and Trp^{14} in several SW Mb complexes (except when indicated). References are in brackets

Myoglobin complex	**Trp7**	**Trp14**
DeoxyMb	105(9)	18(9)
metMb	135(10) 112.5(9)	16(10) 21.5(9)
MbCO	132(10) 125.4(9)	26(10) 23.4(9)
MbCN	113.2(9)	28.5(9)
MbN_3	109.4(9)	27(9)
MbO_2	122(9)	24.4(9)
HH apoMb	2840(11)	2806(11)

SII.2 Data analysis

The white-light super-continuum probe pulses are generated with some chirp and have duration of ~300 fs FWHM. Frequency-resolved detection allows however to correct for a difference of time-zero for different probe frequencies and this does not limit the time-resolution of the experiment.

Global analysis of the time-zero corrected data-matrix $M(\lambda,t)_{m\times n}$ was performed by a Singular Value Decomposition (SVD) technique. The latter is known to reduce the fit dimensionality and to act as a noise filter.(12-14) The SVD procedure starts from the data matrix $M(\lambda,t)_{m\times n}$ and it decomposes the latter in the product of three matrices, as shown in eq. 1:

$$M(\lambda,t) = S(\lambda)_{m\times m} \times W_{m\times n} \times T(t)^{T}{}_{n\times n} \tag{S2}$$

If the data matrix can be described by a discrete linear combination of terms and in the case of pure stochastic noise, the columns present in the $S(\lambda)_{m\times m}$ and $T(t)^{T}{}_{n\times n}$ matrices are known as singular spectra (also called “eigenspectra”) and singular kinetic vectors (also called “eigentraces”) respectively. $W_{m\times n}$ is a matrix that has $w_{ij} = w_{ji} = 0$ while $w_{ii} \neq 0$. The latter entries are also called *“singular values”* and represent the contribution of each eigenspectrum (and the corresponding eigentrace) to the data matrix. In the case of noise-free data there are N non-vanishing singular values, while the presence of noise acts as a perturbation of the latter and the respective singular vectors.(12-14)

A GF analysis of the relevant eigentraces allows retrieving the exponential time constants τ_k with their respective uncertainties and amplitudes a_{ik}. The fitting function used to fit the eigentraces is given by

$$f(t) = H(t) * (G(t) \otimes \sum_i a_i exp^{(-\frac{t}{\tau_i})}) \tag{S3}$$

Where H(t) is the Heaviside step function, G(t) is a Gaussian function with a FWHM equal to the IRF of the measurement and the last part is a sum of exponential functions with a given amplitudes a_i and time constants τ_i.

The amplitudes can then be used to construct the Decay Associated Spectra (DAS), which give the spectral contribution associated to a given time-constant as:

$$DAS_k(\lambda) = \sum_k a_{ik}\, w_{ii}\, U_k(\lambda) \tag{S4}$$

where U_k (λ) is the eigenspectrum related to the *k*-th eigentrace.

The data were analyzed both via GF of single kinetic traces and SVD of the entire data matrix. The results obtained with these methods agree with each other, within the experimental error.

Figure S3 shows the result of the GF of several selected kinetic traces, for 315 nm (A) and 290 nm excitation (B). The best-fit of the kinetic traces, obtained by photo-excitation of deoxy-Mb at 315 nm, gave time-scales of: 280 ± 60 fs, 1.6 ± 0.2 ps and 4.0 ± 0.4 ps. After ~10 ps, the system has completely recovered, except for a very small component due to multi-photon absorption as discussed above.

When deoxy-Mb is excited at 290 nm, a sum of three exponentials is not sufficient. The minimum number of exponentials necessary to best-fit the selected kinetic traces is six, whose associated time-scales are: 230 ± 60 fs, 1.5 ± 0.2 ps, 4.4 ± 0.4 ps, 18 ± 2 ps, 106 ± 10 ps and 5 ns. The last time-constant was fixed and used to account for the unknown lifetime of the LL photo-product, which is longer than our measurement window of 1 ns. Moreover a careful analysis of the kinetic traces shows that, at ~20 ps (Trp[14] relaxation), a small growth of the transient signal can be seen.

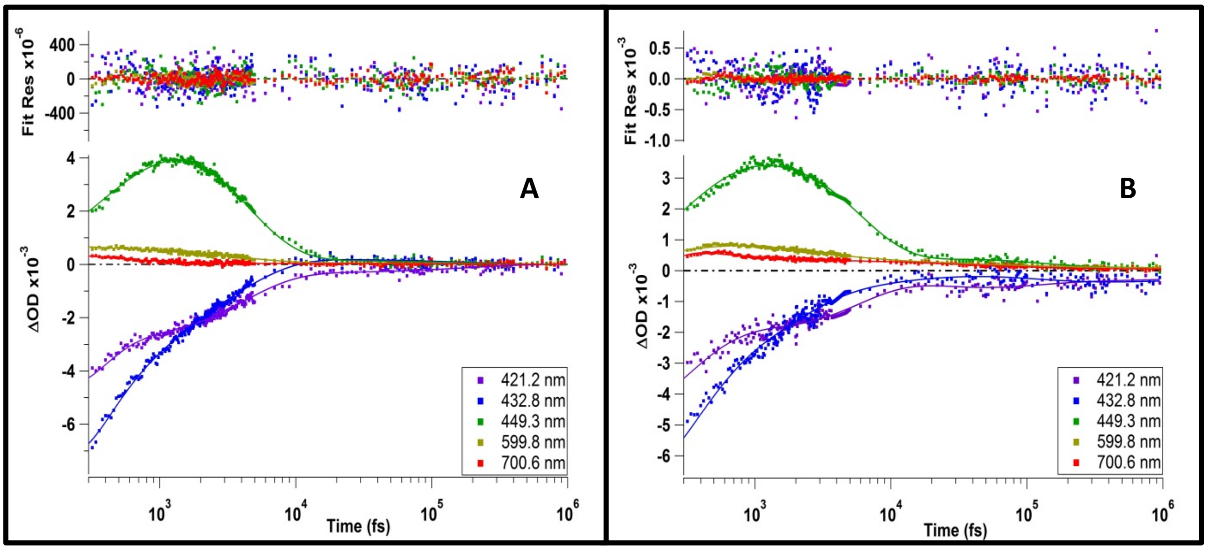

Figure S3 : Selected kinetic traces upon 315 nm excitation (A) and 290 nm excitation (B), along with the global fit traces (solid lines) and their residuals in the upper part.

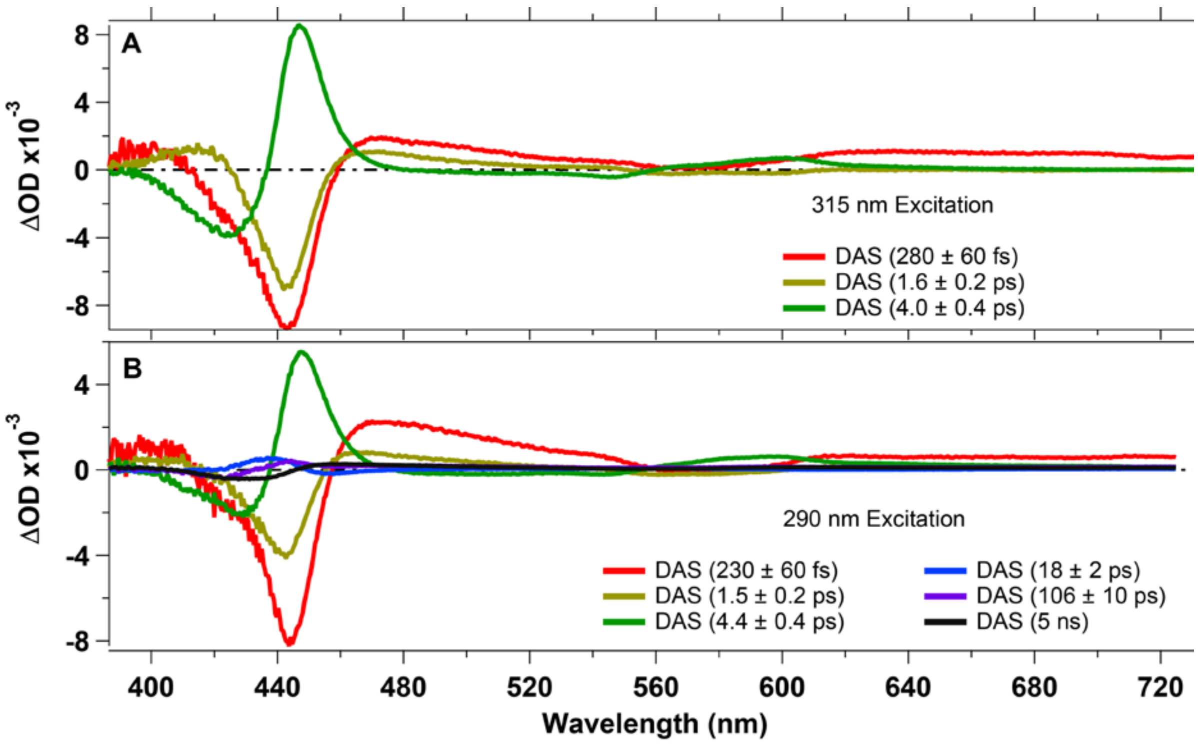

Figure S4: Comparison of the deoxy-Mb DAS's upon 315 nm excitation (A) and 290 nm excitation (B). The color code for the haem dynamics is the same for both the excitation wavelengths.

Similar results were obtained by an SVD analysis, which is presented in Figure S4. The most important DAS are shown in the main paper, here we report the entire set of DAS. As already mentioned in the paper, the 230 fs DAS is not fully reliable since this time-constant is very close to the IRF of the measurement (~300 fs). However it can be seen that a qualitative comparison between the 280 fs DAS (315 nm excitation) and 230 fs DAS (290 nm excitation) shows good agreement. Good agreement is also found for the ~1.6 ps DAS and the ~4 ps DAS's of the two measurements (Figure S4).

To calculate the quantum yield for the photo-product generation we have taken into account an indirect estimation of the total number of molecules undergoing reduction ($\mathrm{Molec_{RED}}$), the total number of excited molecules ($\mathrm{Molec_{EXC.}}$) and the excited Trp^{14} percentage ($\mathrm{Exc_{Trp14}}$). With these three parameters we can obtain the quantum yield for the generation of the photo-reduced species with respect to the total number of excited molecules ($\mathrm{QY_{RED}}$) and with respect to the Trp^{14} ($\mathrm{QY_{ET}}$).

$$QY_{RED.} = \frac{Molec_{RED.}}{Molec_{EXC.}} \qquad QY_{ET} = \frac{QY_{RED.}}{Exc_{Trp14}} \tag{S5}$$

The total number of excited molecules was obtained by summing up all the DAS's and rescaling the absorption spectrum (in the same experimental condition of the measurement) to the Ground State Bleach (GSB) amplitude. A similar procedure was followed to account for the number of molecules undergoing photo-reduction: the spectrum was rescaled to the GSB amplitude of the transient signal at 900 ps. The scaling values obtained for the total number of excited molecules and the number of reduced molecules were found to be: $Molec_{EXC} = 0.0257$ and $Molec_{RED} = 0.00112$. To estimate the number of excited Trp^{14} molecules we have compared the molar extinction coefficient of haem and Trp at 290 nm, finding that the haem accounts for ~70 % of the total absorption and the two Trp account for ~30%. This implies that ~15% of the excited molecules are Trp^{14}, leading to $Exc_{Trp14} = 0.15$. Inserting the numbers in Eq. 5 we can obtain the quantum yield for the total reduction and for the electron transfer process, finding:

$$QY_{RED} = 4.4\% \qquad QY_{ET} = 29\ \%.$$

SII.3 Porphyrin radical anions

Scheme S1 was reproduced from the work of Yamaguchi and Morishima(1) and shows a qualitative representation of the relative energies of the porphyrin and metal orbitals for Fe^{II}-Octaethylporphyrin (OEP) and –Tetraphenylporphyrin (TPP). In their work, Yamaguchi and Morishima(1) reported the influence of the meso- and β-substitution of the porphyrin ring on the energy of its e_g orbitals. The latter is then related to the energy of the *d* orbitals of the metals, leading to the definition of different types of products obtained upon reduction. They synthesized several Fe^{II}-OEP and -TPP derivatives and performed one and two electron reductions for each of them. The latter were characterized by UV-Vis, NMR and ESR spectroscopy, allowing them to gather information on the absorption spectrum related to each species together with the spin state and the molecular structure. With all this information, they could generalize their results, obtaining four categories: 1) four-coordinated Fe^{I} low-spin porphyrin (Type I); 2) five-coordinated Fe^{I} low-spin porphyrin (Type II); 3) four-coordinated Fe^{II} low-spin π-anion radical porphyrin (Type III); 4) five-coordinated Fe^{II} high-spin π-anion radical porphyrin (Type IV).

Scheme S1 shows the orbital energies for the Type II and Type IV, which are relevant to our case. Indeed, a Type I or Type III photo-product, in the Mb case, would imply the detachment of the haem from the protein backbone leading to deterioration of the protein itself.

In Scheme S1**A,** the e_g orbitals of the porphyrin lie at higher energy than the metal *d* orbitals, such that one-electron reduction of [Fe^{II} (CN-OEP)] generates [Fe^{I} (CN-OEP)]$^-$. On the other hand, Scheme S1**B** represents an electronic configuration in which the *Eg* orbitals lie at lower energies than the $d_{x^2-y^2}$ orbital such that one-electron reduction of [Fe^{II} (NO_2-OEP)] generates [Fe^{II} (NO_2-OEP)]$^{\bullet-}$. These two examples show that the modulation of the energy levels on the porphyrin ring, performed by the substituent, can lead to two completely different products. In their work, Yamaguchi and Morishima(1) underlined the importance of the relative energy between the porphyrin e_g orbitals and the metal *d* orbitals. Furthermore, their UV-Vis results can be applied to our results although the type of porphyrin and the solvent used are different (see main paper). As already mentioned in the main paper, in deoxy-Mb the energy difference of the e_g and *d* orbitals is very small, leading to the formation of the Fe^{II} π-anion radical porphyrin.

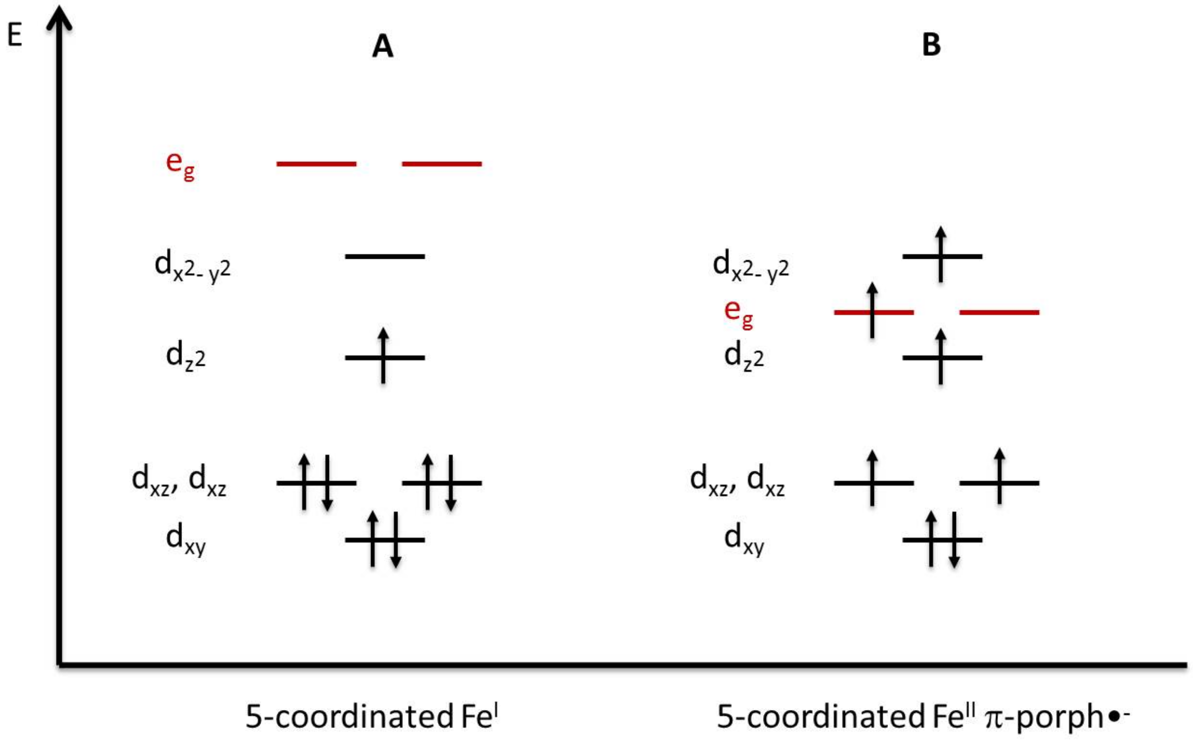

Scheme S1: Schematic representation of relative metal and porphyrin orbital energies for penta-coordinated Fe^{I} (A) and penta-coordinated Fe^{II} porphyrin π-anion radical (B). The Fe d-orbitals are in black while the e_g orbitals of the porphyrin ring are in red. Reproduced from ref. (1)

SII.4 Additional Figures

Here we present a larger set of TA spectra (Figures S5 and S6) than in the main text.

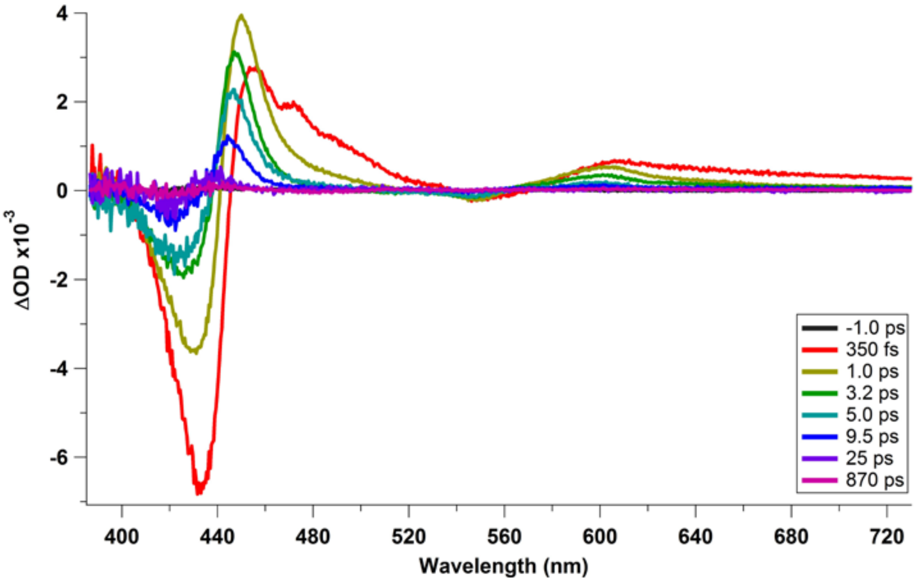

Figure S5: Transient absorption spectra of deoxy-Mb at selected time delays after 315 nm excitation.

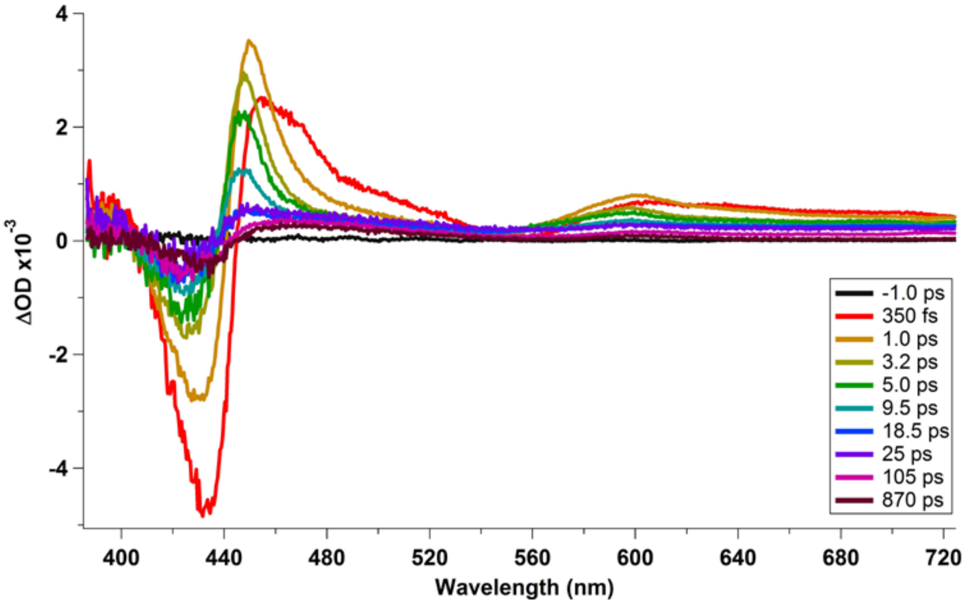

Figure S6: Transient absorption spectra of deoxy-Mb at selected time delays after 290 nm excitation.

Figure S7 (A) shows the structure of the myoglobin (backbone in green) reported from the Protein Data Bank. Here the most important residues for the electron transfer pathway, namely Trp, Leucine (Leu), Valine (Val) and Histidine (His), and the Haem are highlighted. (B) zooms into the most interesting region of Mb, where the Trp^{14} and the Haem are seen along with the two residues through which electron tunneling could occur, namely Leu^{69} and Val^{68}.

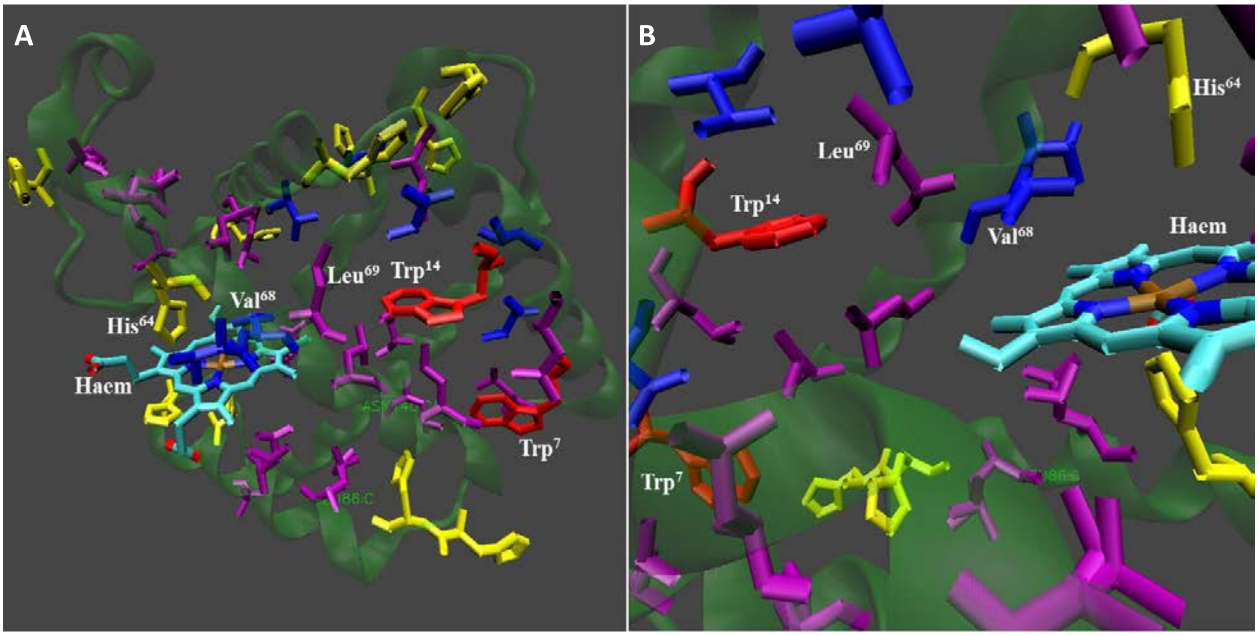

Figure S7: (A) Structure of myoglobin. The backbone is in green, the haem is highlighted by the used of different colors for each atom (namely C, O, N and Fe) and the most important residues for the electron transfer are labeled (Trp in red, Val in blue, Leu in violet and His in yellow). (B) Zoom of the region most relevant for electron transfer showing the residues between Trp and Haem.

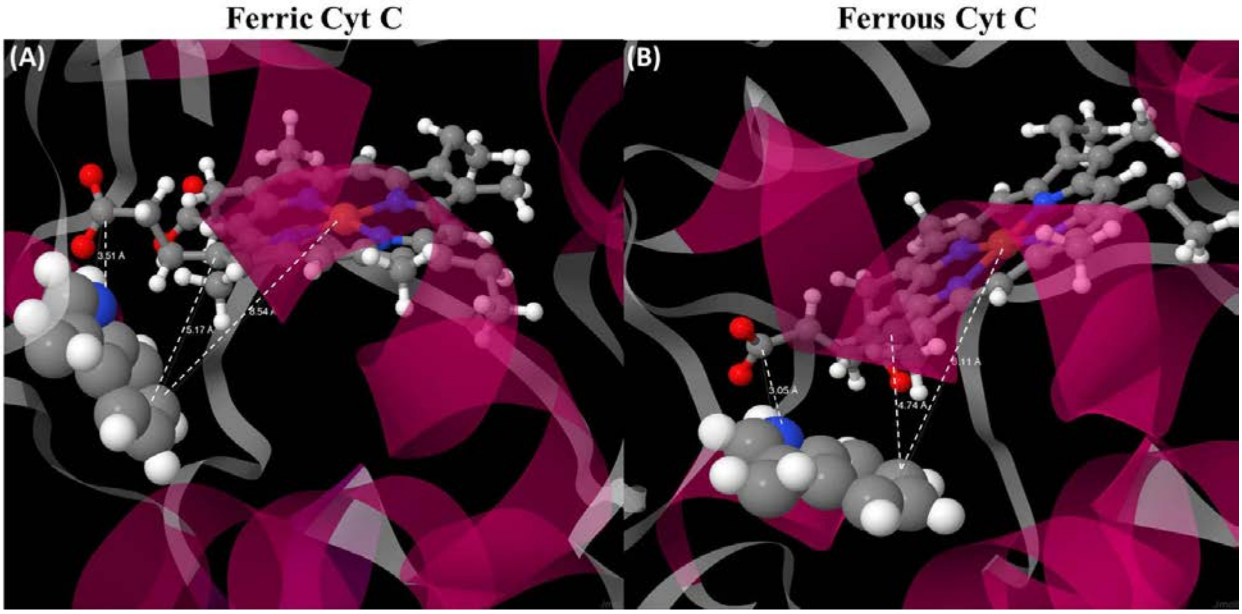

Figure S8: Protein structure of the Cytochrome c in its ferric (A) and ferrous (B) state, displaying distances between the indol-moiety and the haem in both cases. In blue is Nitrogen, in red Oxygen, in gray Carbon and in ochre the Fe.

Figure S8 shows the structures of ferric (A) and ferrous (B) Cytochrome c (Cyt c), with the relevant distances.(15, 16)

References

1. Yamaguchi K & Morishima I (1992) Low-Valent Iron Porphyrins - Nmr Evidence for Pi-Anion-Radical Character in 2-Electron-Reduced Iron(Iii) Mesosubstituted or Beta-Pyrrole-Substituted Porphyrins. *Inorg Chem* 31(15):3216-3222.
2. Aubock G*, et al.* (2012) Femtosecond pump/supercontinuum-probe setup with 20 kHz repetition rate. *Rev Sci Instrum* 83(9).
3. Aubock G, Consani C, van Mourik F, & Chergui M (2012) Ultrabroadband femtosecond two-dimensional ultraviolet transient absorption. *Optics Letters* 37(12):2337-2339.
4. Gouterman M (1961) Spectra of Porphyrins. *J Mol Spectrosc* 6(1):138-&.
5. Fukuda TaK, N. (2010) Electronic absorption spectra-Phtalocyanines. *Handbook of Porphyrin Science*, ed Kadish KM, Smith, K.M. and Guilard, R. (World Scientific), Vol 9.
6. Kuriyan J, Wilz S, Karplus M, & Petsko GA (1986) X-Ray Structure and Refinement of Carbon-Monoxy (Fe-Ii)-Myoglobin at 1.5-a Resolution. *J Mol Biol* 192(1):133-154.
7. Evans SV & Brayer GD (1988) Horse Heart Metmyoglobin - a 2.8-a Resolution 3-Dimensional Structure Determination. *Journal of Biological Chemistry* 263(9):4263-4268.
8. Lakowicz JR (2004) Protein Fluorescence. *Principles of Fluorescence Spectroscpy*, (Springer, U.S.), second Ed, pp 446-480.
9. Willis KJ, Szabo AG, Zuker M, Ridgeway JM, & Alpert B (1990) Fluorescence Decay Kinetics of the Tryptophyl Residues of Myoglobin - Effect of Heme Ligation and Evidence for Discrete Lifetime Components. *Biochemistry-Us* 29(22):5270-5275.
10. Hochstrasser RM & Negus DK (1984) Picosecond Fluorescence Decay of Tryptophans in Myoglobin. *P Natl Acad Sci-Biol* 81(14):4399-4403.
11. Glandieres JM, Twist C, Haouz A, Zentz C, & Alpert B (2000) Resolved fluorescence of the two tryptophan residues in horse apomyoglobin. *Photochem Photobiol* 71(4):382-386.
12. Galo AL & Colombo MF (2013) Singular Value Decomposition and Ligand Binding Analysis. *J Spectrosc*.
13. Henry ER (1997) The use of matrix methods in the modeling of spectroscopic data sets. *Biophys J* 72(2):652-673.
14. Ruckebusch C, Sliwa M, Pernot P, de Juan A, & Tauler R (2012) Comprehensive data analysis of femtosecond transient absorption spectra: A review. *J Photoch Photobio C* 13(1):1-27.
15. Banci L, Bertini I, Huber JG, Spyroulias GA, & Turano P (1999) Solution structure of reduced horse heart cytochrome c. *Journal of biological inorganic chemistry : JBIC : a publication of the Society of Biological Inorganic Chemistry* 4(1):21-31.
16. Banci L*, et al.* (1997) Solution structure of oxidized horse heart cytochrome c. *Biochemistry* 36(32):9867-9877.